GaN-Based T-Type Totem-Pole Rectifier with ZVS Control and Reactive Power Regulation

Jingjing Sun
Min H. Kao Department of Electrical Engineering and Computer Science
The University of Tennessee
Knoxville, TN, USA
jsun30@vols.utk.edu

Liyan Zhu
Min H. Kao Department of Electrical Engineering and Computer Science
The University of Tennessee
Knoxville, TN, USA
lzhu21@vols.utk.edu

Ruiyang Qin
Min H. Kao Department of Electrical Engineering and Computer Science
The University of Tennessee
Knoxville, TN, USA
rqin1@vols.utk.edu

Jie Li
Min H. Kao Department of Electrical Engineering and Computer Science
The University of Tennessee
Knoxville, TN, USA
jli94@vols.utk.edu

Daniel J. Costinett
Min H. Kao Department of Electrical Engineering and Computer Science
The University of Tennessee
Knoxville, TN, USA
daniel.costinett@vols.utk.edu

Leon M. Tolbert
Min H. Kao Department of Electrical Engineering and Computer Science
The University of Tennessee
Knoxville, TN, USA
tolbert@utk.edu

2022 IEEE Energy Conversion Congress and Exposition (ECCE) | 978-1-7281-9387-8/22/$31.00 ©2022 IEEE | DOI: 10.1109/ECCE50734.2022.9947608

***Abstract*—This paper proposes a high-efficiency single-phase GaN-based T-type totem-pole front-end rectifier with reactive power transfer. A full-range zero voltage switching (ZVS) modulation approach for both unity power factor (PF) operation and non-unity PF operation is proposed for the GaN-based rectifier in critical conduction mode (CRM) operation. T-type mode operation and switching frequency limitation are proposed to overcome the ac-line zero-crossing challenges. A digital-based control strategy is also proposed to regulate the active power and reactive power simultaneously. A 1.6 kVA prototype of the T-type totem-pole rectifier is built and demonstrated with full-range ZVS operation, 98.9% full-load efficiency, and flexible reactive power regulation.**

***Index Terms*—GaN, rectifier, CRM, ZVS, soft switching, reactive power compensation**

I. Introduction

Reactive power compensation is important for improving the grid power quality [1]–[3]. Traditional power compensators like static VAR compensator (SVC) and static synchronous compensator (STATCOM) have been widely used for providing flexible power compensation [4], [5]. However, centralized power compensators are bulky, expensive, and exhibit large power loss [6], [7]. On the other hand, grid support with load participation is a cost-effective approach to manage the power grid [8]. Advantageous in large power consumption and flexible loading, critical loads like data centers and telecommunication power supplies can also provide fast reactive power compensation with their front-end rectifiers [9], [10].

Research efforts have been made on using single-phase grid-connected converters for reactive power compensation [9]–[16]. Due to the characteristic of diode unidirectional current flow, diode-based rectifiers suffer from severe input current distortion and limited capability of reactive power compensation [13], [14]. Active front-end rectifiers, such as MOSFET-based full-bridge pulse-width modulation (PWM) converter and totem-pole power factor correction (PFC) rectifier, allow bidirectional power flow and are able to transfer reactive power with wide power factor range and low input current distortion [9], [10], [15], [16]. In [9], a bidirectional rectifier with active and reactive power regulation was developed for telecommunication application. In [15], a full-bridge single-phase rectifier was designed for an on-board plug-in EV charger that can provide reactive power support to the grid in addition to charging the vehicle battery.

However, existing work on the single-phase rectifier with reactive power operation concentrates on Si-based hard-switching PWM converters, which have low efficiency and low power density. Recently, GaN-based totem-pole power factor correction (PFC) rectifier with critical conduction mode (CRM) and zero voltage switching (ZVS) control has been demonstrated with high power density and high efficiency (99% peak efficiency) [17], [18]. If extending the rectifier into two-quadrant operation, both active power transfer and reactive power regulation are realized with high efficiency, and the expensive bulky centralized power compensator may be saved.

Fig. 1 shows the topology of a GaN-based CRM totem-pole rectifier that operates in unipolar modulation and is able to perform reactive power transfer. However, challenges appear during the ac-line zero-crossing regions. First, high peak switching frequency occurs at the ac current zero-crossing [19]. This is because the zero-crossing points of i_{in} and v_{in} are no longer at the same moment with the phase

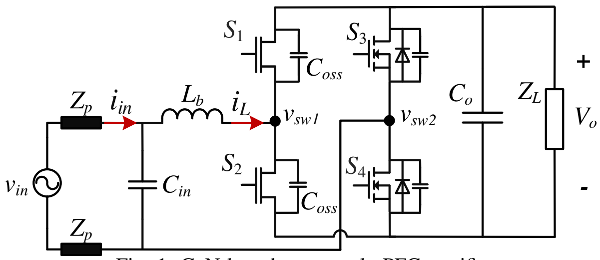

Fig. 1. GaN-based totem-pole PFC rectifier.

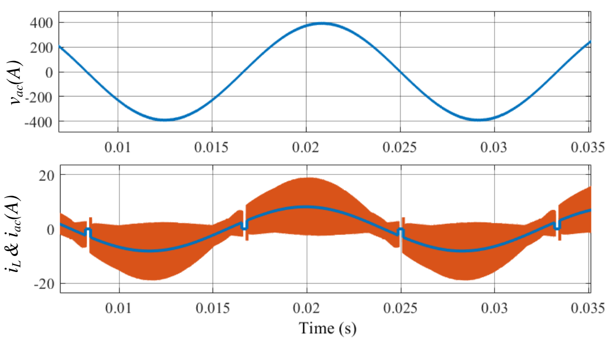

Fig. 2. Simulation waveforms of the CRM totem-pole rectifier at 0.94 leading PF with 200 μs blanking time during the ac voltage zero-crossing when $v_{in} = 277\ \mathrm{V_{ac}}, V_o = 480\ \mathrm{V_{dc}}, P = 1.5\ \mathrm{kW}, Q = -500\ \mathrm{VAr}$.

shift in non-unity PF. During the ac current zero-crossing, v_{in} is not zero, leading to very high switching frequency to maintain the CRM operation. The peak switching frequency further increases with higher reactive power and lower PF, resulting in high switching loss and gate drive loss.

Second, during the ac voltage zero-crossing, a large current spike or even instability occurs when v_{in} polarity does not match with the Si device switching due to sensing error or switching noise [18], [20]. Typically, a blanking time (around 200 μs) is adopted to achieve a stable zero-crossing transition [21]. Nevertheless, the blanking-time approach is not applicable in the case with reactive power operation. As shown in Fig. 2, when i_{in} is not in phase with v_{in}, blanking time during v_{in} zero crossing results in severe i_{in} distortion, which is unacceptable for a front-end rectifier. Currently, no work studies the detailed design of a GaN-based CRM rectifier with soft switching and reactive power transfer. Also, an effective method for overcoming the implementation challenges during ac line zero-crossing has not been provided.

This paper proposes a single-phase GaN-based T-type totem-pole rectifier that achieves full-range ZVS operation for high efficiency, simultaneous active power and reactive power transfer, and overcomes the challenges during ac line zero crossing. The paper is organized as follows. Section II introduces the proposed the GaN-based T-type totem-pole rectifier with full-range ZVS modulation and peak frequency limitation. Section III presents the control strategy for active power and reactive power regulation. Section IV shows the experimental verification, and Section V gives the conclusions.

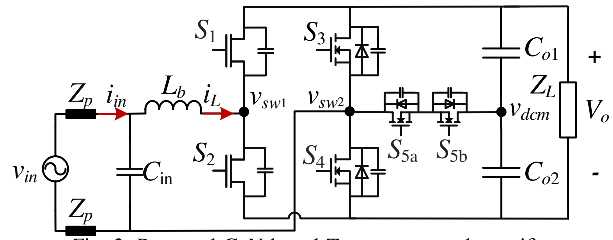

Fig. 3. Proposed GaN-based T-type totem-pole rectifier.

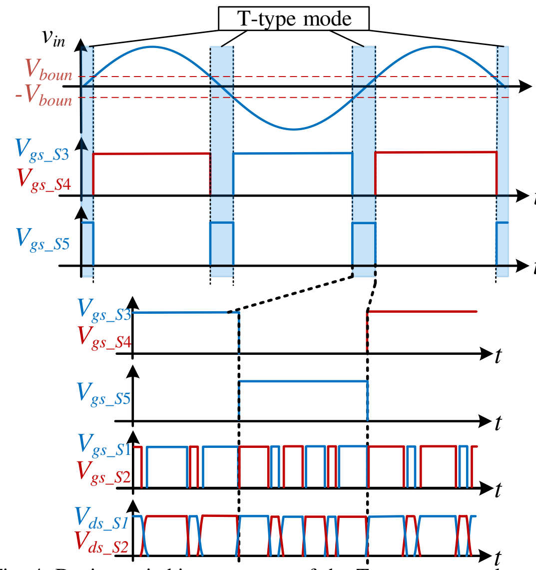

Fig. 4. Device switching sequence of the T-type totem-pole rectifier.

II. Proposed GaN-based CRM Rectifier with Full-Range ZVS Modulation

A. Proposed CRM T-type Totem-Pole Rectifier

Fig. 3 shows the proposed GaN-based rectifier. Compared to the conventional totem-pole rectifier, a bidirectional switch S_5 that is composed of two anti-series connected Si MOSFETs S_{5a}, S_{5b} is inserted between the Si phase leg and the dc capacitor. Since a T-type structure is constructed, the topology is called T-type totem-pole rectifier.

The rectifier has two operation modes: totem-pole mode and T-type mode. Fig. 4 illustrates the device switching pattern of the T-type totem-pole rectifier. An intermediate boundary voltage V_{boun} is defined to distinguish the two operation modes. When $|V_{in}| > V_{boun}$, the rectifier operates in the normal totem-pole mode with unipoloar modulation. Bidirectional switch S_5 is OFF, S_3 conducts during the negative half cycle, and S_4 conducts during the positive half cycle. When $|V_{in}| \leq V_{boun}$, the rectifier operates in T-type mode with S_5 ON and S_3, S_4 OFF. The boost inductor is charged with $v_L = V_{in} + 0.5V_o > 0$ when S_2 conducts and discharged with $v_L = V_{in} - 0.5V_o < 0$ when S_1 is ON. In this way, the inductor voltage is dominated by the output voltage and is always under control during the V_{in} zero-crossing. By adopting the T-type mode, Si MOSFETs' switching is independent of v_{in} zero-crossing detection, and the instability condition and current distortion during the voltage zero-crossing are avoided.

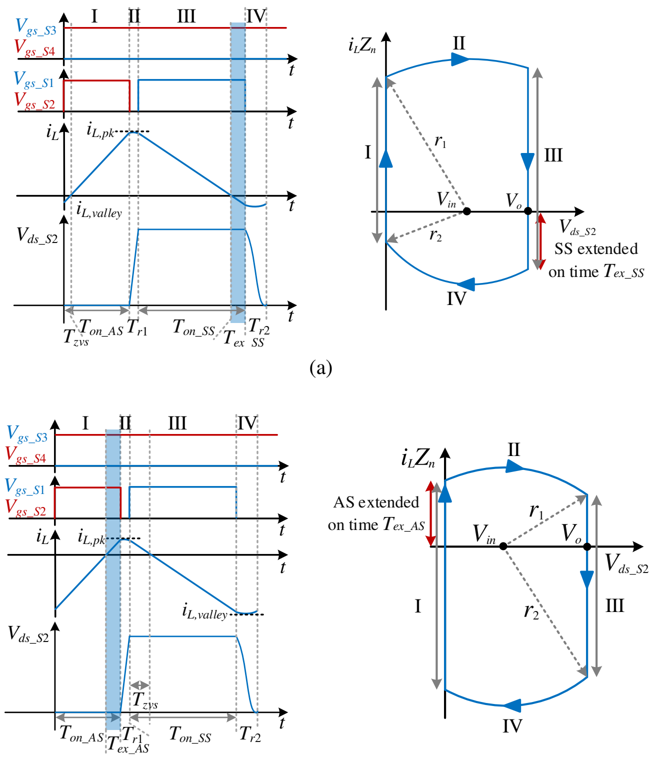

(a)

(b)

Fig. 5. ZVS waveforms and state plane trajectory during totem-pole mode when (a) $V_{in} > 0, I_{in} > 0$; (b) $V_{in} > 0, I_{in} < 0$.

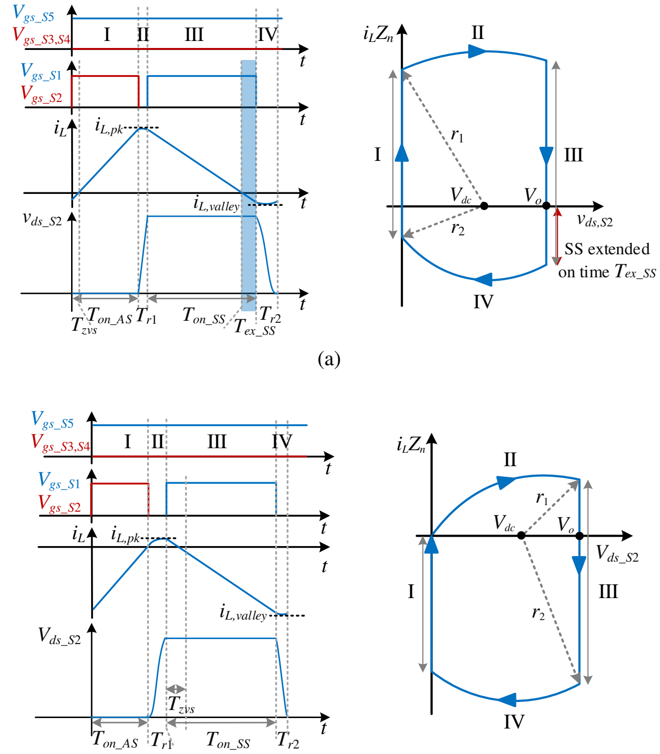

(a)

(b)

Fig. 6. ZVS waveforms and state plane trajectory during T-type mode when (a) $V_{in} > 0, I_{in} > 0$; (b) $V_{in} > 0, I_{in} < 0$.

B. Proposed Full-Range ZVS Modulation

The rectifier is designed to achieve full-range ZVS turn-ON of GaN devices in unity PF operation and non-unity PF operation. To analyze the operation principle, the rectifier waveforms and state-plane trajectories within one switching cycle are illustrated. Due to the symmetric characteristic, the following discussion will only consider the positive half-line cycle of the input voltage, and assumes that the input voltage remains constant within one switching cycle. For the state-plane trajectories, the characteristic impedance Z_n is defined as $Z_n^2 = {}^{L_b}/_{(2C_{oss})}$, where C_{oss} is the equivalent drain-to-source capacitance of S_1 and S_2, assuming $C_{oss,S1} = C_{oss,S2} = C_{oss}$.

1) ZVS Modulation during Totem-Pole Mode

During the totem-pole mode with S_5 OFF, the rectifier operates in the same way as the conventional CRM totem-pole PFC rectifier [22]. When $V_{in} > 0, I_{in} > 0$ (Fig. 5(a)), synchronous switch (SS) device S_1 turns on naturally with ZVS, but active switch (AS) device S_2 can only achieve ZVS when $V_{in} \leq V_o$. To also realize ZVS when $V_{in} > 0.5V_o$, the conduction time of SS device, T_{on_SS}, is extended by T_{ex_SS}. When $V_{in} > 0, I_{in} < 0$ (Fig. 5(b)), S_2 achieves ZVS turn-ON passively since $|i_{L,valley}|$ is large enough to discharge $C_{oss,S2}$. However, S_1 only realizes valley switching when $V_{in} < 0.5V_o$. To achieve S_1 ZVS turn-ON, the conduction time of S_2, T_{on_AS}, is extended by T_{ex_AS} for a larger $|i_{L,pk}|$. Table I summarizes the key modeling parameters for ZVS modulation in the four quadrants of V_{in} and I_{in}. k is the full-range ZVS constraint defined as $k = {}^{r_2}/_{V_{in}}$ when $I_{in} > 0$ and $k = {}^{r_1}/_{V_{in}}$ when $I_{in} < 0$, and k_0 is the ZVS margin coefficient that is slightly larger than 1, as illustrated in [22]. k_{lim} is the coefficient for peak frequency limitation, which is illustrated in Section II-C.

2) ZVS Modulation during T-Type Mode

To maintain the full-range ZVS operation, ZVS modulation during the T-type mode is also proposed. Fig. 6 presents the switching waveforms and state-plane trajectories during the T-type mode with positive v_{in}. When $V_{in} > 0$, $I_{in} > 0$ (Fig. 6(a)), S_1 realizes ZVS naturally, but S_2 can only achieve valley switching because $(|V_{in}|+0.5V_o) \geq 0.5V_o$ and $|i_{L,valley}|$ is not large enough to discharge $C_{oss,S2}$. Therefore, ZVS extension is required by increasing the conduction time of S_1 to increase $|i_{L,valley}|$ and gain more inductor energy for the resonance. When $V_{in} > 0, I_{in} < 0$ (Fig. 6(b)), both GaN devices can achieve ZVS turn-ON naturally and ZVS extension is not required. Considering the peak switching frequency limitation, ZVS operation principle during the T-type mode is summarized in Table II.

C. Peak Frequency Limitation

A frequency limitation method is proposed to reduce the peak switching frequency by modifying the ZVS margin constraint k. To simplify the calculation of switching period t_{sw}, the inductor current is approximated as a triangular waveform with linear increase from $i_{L,valley}$ to $i_{L,pk}$ and linear decrease

TABLE I. ZVS operation principle of the GaN-based CRM T-type totem-pole rectifier during totem-pole mode.

Positive half-line cycle of the input voltage		
Parameter	$V_{in} > 0, I_{in} > 0$	$V_{in} > 0, I_{in} < 0$
Active switch (AS)	S_2	S_2
Synchronous switch (SS)	S_1	S_1
AS natural ZVS region	$V_{in} \le V_{bound,zvs}, \quad V_{bound,zvs} = \frac{V_o}{k_0+1}$	all range
SS natural ZVS region	all range	$V_{in} \ge V_{bound,zvs}, \quad V_{bound,zvs} = \frac{k_0 V_o}{k_0+1}$
ZVS constraint	$k = \begin{cases} \max\{k_{lim}, \frac{V_o - V_{in}}{V_{in}}\}, V_{in} \le V_{bound,zvs} \\ \max\{k_{lim}, k_0\}, \qquad V_{in} > V_{bound} \end{cases}$	$k = \begin{cases} \max\{k_{lim}, \frac{V_{in}}{V_o - V_{in}}\}, V_{in} \ge V_{bound,zvs} \\ \max\{k_{lim}, k_0\}, \qquad V_{in} < V_{bound} \end{cases}$
Extended ON time	$T_{ex\_SS} = \frac{\sqrt{(k^2-1)V_{in}^2 - V_o^2 + 2V_o V_{in}}}{w_r(V_o - V_{in})}$	$T_{ex\_AS} = \frac{\sqrt{(k^2-1)V_{in}^2 + V_o^2 - 2V_o V_{in}}}{w_r V_{in}}$
Negative half-line cycle of the input voltage		
Parameter	$V_{in} < 0, I_{in} > 0$	$V_{in} < 0, I_{in} < 0$
Active switch (AS)	S_1	S_1
Synchronous switch (SS)	S_2	S_2
AS natural ZVS region	all range	$-V_{in} \le V_{bound,zvs}, \quad V_{bound,zvs} = \frac{V_o}{k_0+1}$
SS natural ZVS region	$-V_{in} \ge V_{bound,zvs}, \quad V_{bound,zvs} = \frac{k_0 V_o}{k_0+1}$	all range
ZVS constraint	$k = \begin{cases} \max\{k_{lim}, \frac{-V_{in}}{V_o + V_{in}}\}, -V_{in} \ge V_{bound,zvs} \\ \max\{k_{lim}, k_0\}, \qquad -V_{in} < V_{bound} \end{cases}$	$k = \begin{cases} \max\{k_{lim}, \frac{V_{in} + V_o}{-V_{in}}\}, -V_{in} \le V_{bound,zvs} \\ \max\{k_{lim}, k_0\}, \qquad -V_{in} > V_{bound} \end{cases}$
Extended ON time	$T_{ex\_SS} = \frac{\sqrt{(k^2-1)V_{in}^2 + V_o^2 + 2V_o V_{in}}}{-w_r V_{in}}$	$T_{ex\_AS} = \frac{\sqrt{(k^2-1)V_{in}^2 - V_o^2 - 2V_o V_{in}}}{w_r(V_o + V_{in})}$

TABLE II. ZVS operation principle of the GaN-based CRM T-type totem-pole rectifier during T-type mode.

Positive half-line cycle of the input voltage		
Parameter	$V_{boun} \ge V_{in} > 0, I_{in} > 0$	$V_{boun} \ge V_{in} > 0, I_{in} < 0$
Active switch (AS)	S_2	S_2
Synchronous switch (SS)	S_1	S_1
AS natural ZVS region	no range	all range
SR natural ZVS region	all range	all range
Full-range ZVS constraint	$k = \max\{k_0, k_{lim}\}$	$k = \max\{1, k_{lim}\}$
Extended ON time	$T_{ex\_SS} = \frac{\sqrt{k^2(V_{in}+0.5V_o)^2 - (0.5V_o - V_{in})^2}}{w_r(0.5V_o - V_{in})}$	$T_{ex\_AS} = 0$
Negative half-line cycle of the input voltage		
Parameter	$-V_{boun} \le V_{in} < 0, I_{in} > 0$	$-V_{boun} \le V_{in} < 0, I_{in} < 0$
Active switch (AS)	S_1	S_1
Synchronous switch (SS)	S_2	S_2
AS natural ZVS region	all range	no range
SR natural ZVS region	all range	all range
Full-range ZVS constraint	$k = \max\{1, k_{lim}\}$	$k = \max\{k_0, k_{lim}\}$
Extended ONn time	$T_{ex\_AS} = 0$	$(T_{ex\_SS} = \frac{\sqrt{k^2(-V_{in}+0.5V_o)^2 - (0.5V_o + V_{in})^2}}{w_r(0.5V_o + V_{in})}$

from $i_{L,pk}$ to $i_{L,valley}$. Thus, the switching period is expressed as

$$t_{sw} = \frac{1}{f_{sw}} \approx L_b \frac{i_{L,pk} - i_{L,valley}}{v_{L,rise}} + L_b \frac{i_{L,pk} - i_{L,valley}}{-v_{L,fall}} \quad (1)$$

where $v_{L,rise} > 0, v_{L,fall} < 0$ are the voltages applied on the inductor during i_L rising and falling.

Assume f_{smax} is the allowable maximum switching frequency, f_s should be lower than f_{smax}, that is

$$t_{sw} \ge \frac{1}{f_{smax}} \quad (2)$$

Combining (1) and (2), the required inductor current ripple is

$$i_{L,pk} - i_{L,valley} \ge \frac{-v_{L,rise} v_{L,fall}}{L_b f_{smax}(v_{L,rise} - v_{L,fall})} \quad (3)$$

Since $i_{L,pk} + i_{L,valley} = 2i_{L,ave} \approx 2i_{in}$, together with (3),

TABLE III. ZVS constraint limitation k_{lim} for peak frequency limitation of the CRM totem-pole rectifier.

Positive half-line cycle of the input voltage		
	$V_{in} > 0, I_{in} > 0$	$V_{in} > 0, I_{in} < 0$
k_{lim}	$(I_{in} + \frac{V_{L,rise}V_{L,fall}}{2L_b f_{smax}(V_{L,rise}-V_{L,fall})})\frac{Z_n}{-V_{L,rise}}$	$(I_{in} - \frac{V_{L,rise}V_{L,fall}}{2L_b f_{smax}(V_{L,rise}-V_{L,fall})})\frac{Z_n}{-V_{L,fall}}$
Negative half-line cycle of the input voltage		
	$V_{in} < 0, I_{in} > 0$	$V_{in} < 0, I_{in} < 0$
k_{lim}	$(I_{in} - \frac{V_{L,rise}V_{L,fall}}{2L_b f_{smax}(V_{L,rise}-V_{L,fall})})\frac{Z_n}{-V_{L,fall}}$	$(I_{in} + \frac{V_{L,rise}V_{L,fall}}{2L_b f_{smax}(V_{L,rise}-V_{L,fall})})\frac{Z_n}{-V_{L,rise}}$

the inductor current limit is

$$i_{L,pk} \geq i_{in} + \frac{-v_{L,rise}v_{L,fall}}{2L_b f_{smax}(v_{L,rise} - v_{L,fall})} \tag{4}$$

or

$$i_{L,valley} \leq i_{in} - \frac{-v_{L,rise}v_{L,fall}}{2L_b f_{smax}(v_{L,rise} - v_{L,fall})} \tag{5}$$

When $i_{in} > 0$, $i_{L,valley} = -{}^{kv_{rise}}/_{Z_n}$. Inserting $i_{L,valley}$ into (5), the ZVS constraint k is solved. Similar analysis is also applied for the negative half cycle, and Table III summarizes the required k for peak frequency limitation in the four quadrants of V_{in} and I_{in}. Fig. 7 shows the analytical waveforms of a CRM T-type totem-pole rectifier at half load with and without frequency limitation. The peak switching frequency is limited to 800 kHz in Fig. 7(b).

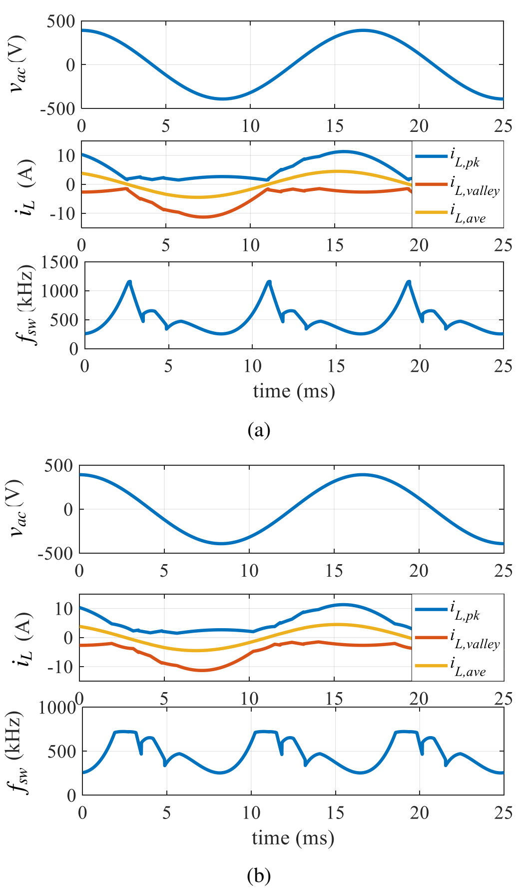

Fig. 7. Analytical waveforms of the CRM T-type totem-pole PFC rectifier at 0.79 leading PF when $V_{in} = 277$ $\mathrm{V_{ac}}, V_o = 480$ $\mathrm{V_{dc}}, L_b = 21$ μH, $V_{boun} = 100$ V, $P = 750$ W,$Q = -600$ kVAr. (a) Peak frequency has no limitation; (b) Peak frequency is limited at 800 kHz.

III. Control Implementation

The proposed control strategy for the T-type totem-pole rectifier is shown in Fig. 8. To control the active power P and reactive power Q separately, instantaneous P and Q are estimated by using the second-order generalized integrator orthogonal signal generator (SOGI OSG) and Park transformation based on the sensed input current and voltage. The input voltage magnitude V_m and phase angle θ are detected in a phase locked loop (PLL), and a conditioned input voltage signal $v_{ac,PLL} = V_m \cos\theta$ is generated for the following control actions.

The output voltage loop with a PI compensator in d-axis regulates the output voltage and active power, and produces the d-axis current reference i_{dref}. In the q-axis, the conditioned reactive power Q is used to form a reactive power loop. Q is adjusted to follow the power reference Q_{ref} by a PI compensator, which generates the q-axis current reference

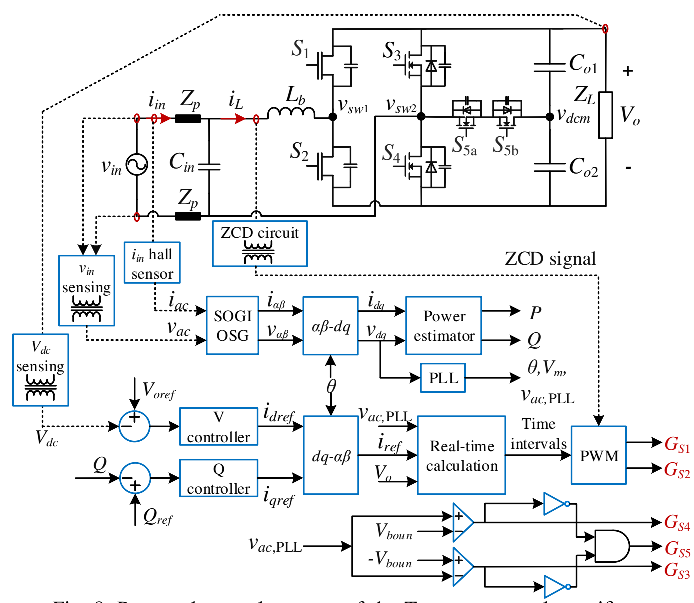

Fig. 8. Proposed control strategy of the T-type totem-pole rectifier.

i_{qref}. The single-phase current reference i_{ref} is formed by i_{dref} and i_{qref}. Then, the current reference together with the conditioned input and output voltages are transmitted to the real-time calculation, where instantaneous switching time intervals are calculated based on the analytical model for full-range ZVS with reactive power operation. Gate signals of the GaN devices S_1, S_2 are synchronized by the sensed inductor zero current detection (ZCD) signal.

On the other hand, line-cycle switched Si MOSFETs are controlled according to the conditioned input voltage $v_{ac,PLL}$. With a defined boundary voltage V_{boun}, S_5 is turned ON to conduct the T-type mode when $|V_{ac,PLL}| \leq V_{boun}$. Otherwise, totem-pole mode is adopted, where S_3 conducts during the negative half cycle when $v_{ac,PLL} < -V_{boun}$, and S_4 conducts during the positive half cycle when $v_{ac,PLL} > V_{boun}$.

IV. Experimental Verification

To verify the design, a single-phase GaN-based CRM T-type totem-pole rectifier prototype is built and tested. Fig. 9 shows the physical prototype, and Table IV summarizes the detailed converter specifications. The rectifier main circuit is enclosed in a $90\ \mathrm{mm} \times 200\ \mathrm{mm} \times 43\ \mathrm{mm}$ space, which is composed of the input EMI filter, boost inductor, GaN and Si devices, gate drive circuits, sensing circuits, auxiliary power supply, and the dc-link capacitors. A TMS320F28379D DSP launchpad from Texas Instruments is used as the controller.

TABLE IV. Specifications of the GaN-based rectifier prototype.

Parameter	Value
Input voltage v_{in}	$277\ \mathrm{V_{ac}}, 60$ Hz
Output voltage V_o	$480\ \mathrm{V_{dc}}$
Active power rating P_o	1.5 kW
Apparent power rating S	1.6 kVA
Switching frequency f_{sw}	$170 - 800$ kHz
GaN devices S_1, S_2	GS66516T, 650 V, 60 A
Si devices S_3, S_4, S_5	IPW65R019C7, 650 V
Boost inductor	21 µH, core Mix-2-T106
Dc-link capacitor	900 µF, ELH687M400AT4AA
ZVS margin	$k_0 = 1.1$, $T_{ZVS,min} = 50$ ns

Fig. 10 and Fig. 11 show the experimental waveforms of the GaN-based CRM T-type totem-pole rectifier prototype at full load with near unity PF. The input current is well regulated in phase with the input voltage, and the output voltage is converted to a stable $480\ \mathrm{V_{dc}}$. Full-range ZVS operation is achieved in both the totem-pole mode and T-type mode, and the tested full-load efficiency is 98.9% at unity PF.

Steady-state operation with different PFs is also demonstrated on the prototype. Table V summarizes the measured operation performance at full load, and Table VI lists the measured operation performance at half load. The tested efficiency at full load and half load is above 98.5%, and the input current THD is below 5%.

Fig. 12 presents the experimental waveforms of the GaN-based T-type totem-pole rectifier at full load with 0.94 lagging PF (Fig. 12(a)), at half load with 0.79 leading PF (Fig. 12(b)),

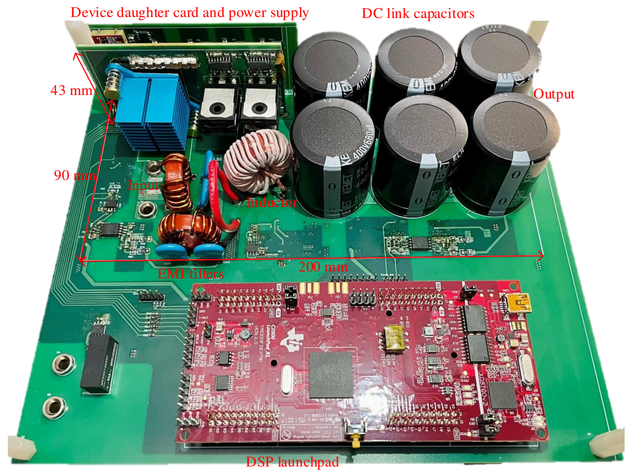

Fig. 9. Proposed control strategy of the T-type totem-pole rectifier.

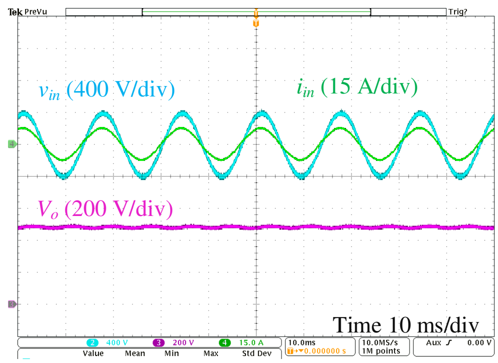

(a) Waveforms of v_{in}, i_{in}, V_o.

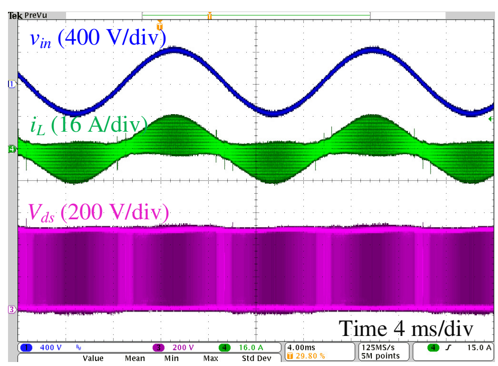

(b) Waveforms of v_{in}, i_L, V_{ds}.

Fig. 10. Full-load experimental waveforms of the GaN-based CRM T-type totem-pole rectifier at unity PF when $v_{in} = 277\ \mathrm{V_{ac}}, V_o = 480\ \mathrm{V_{dc}}$.

TABLE V. Operation performance of the rectifier prototype at full load.

	P (W)	Q (VAr)	PF	η	iTHD
Near unity	1430	-166	> 0.99	98.9%	3.2%
Leading	1437	-499	0.94	98.8%	2.3%
Lagging	1435	516	0.94	98.6%	4.7%

and at half load with 0.87 lagging PF (Fig. 12(c)). With the reactive power closed-loop control, the reactive power and phase shift between v_{in} and i_{in} are regulated accurately. More

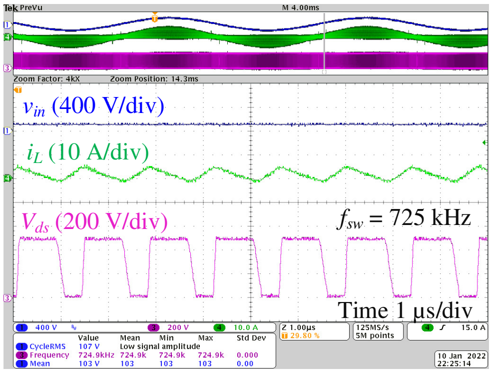

(a) Waveforms of v_{in}, i_L, V_{ds} at during T-type mode.

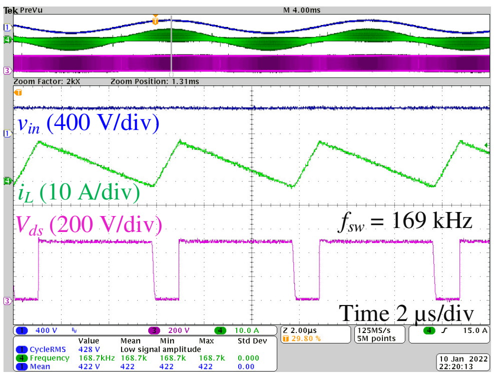

(b) Waveforms of v_{in}, i_L, V_{ds} during totem-pole mode.

Fig. 11. Full-load switching waveforms of the GaN-based CRM T-type totem-pole rectifier at unity PF when $v_{in} = 277\ \mathrm{V_{ac}}, V_o = 480\ \mathrm{V_{dc}}$.

TABLE VI. Operation performance of the rectifier prototype at half load.

	P (W)	Q (VAr)	PF	η	iTHD
Near unity	777	-93	> 0.99	98.7%	4.9%
Leading	782	-600	0.79	98.6%	3%
Lagging	779	431	0.87	98.54%	4.9%

detailed illustration can be found in [23].

V. Conclusions

This article proposes a single-phase GaN-based rectifier with full-range ZVS operation and reactive power transfer capability. To overcome the ac-line zero-crossing challenges of the conventional GaN-based totem-pole PFC rectifier, a T-type totem-pole rectifier is proposed, where a bidirectional switch is added to modify the converter's modulation during the voltage zero-crossing region. A full-range ZVS modulation with peak frequency limitation is proposed to realize GaN devices' ZVS turn-ON at both unity PF operation and non-unity PF operation. Also, a digital-based control strategy with separate power control loops and model-based real-time calculation is developed. The proposed topology, ZVS modulation, and control scheme are verified experimentally on a 1.6 kVA GaN-based rectifier prototype. Full-range ZVS turn-ON of GaN devices are achieved, and the measured full-load efficiency of the rectifier at unity PF is 98.9%. Reactive power transfer

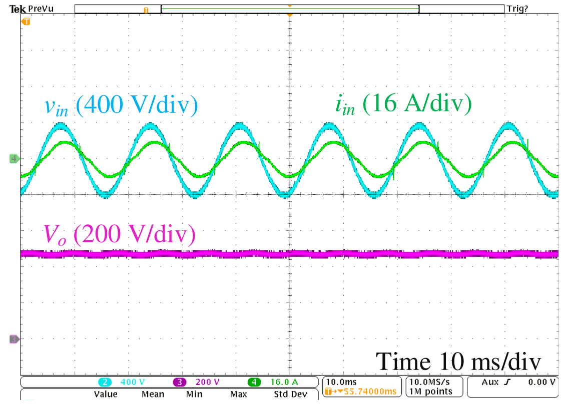

(a)

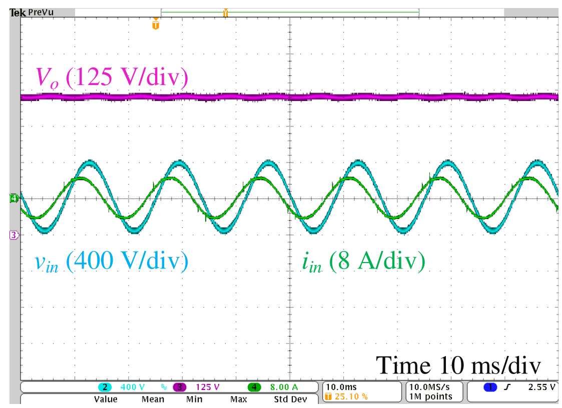

(b)

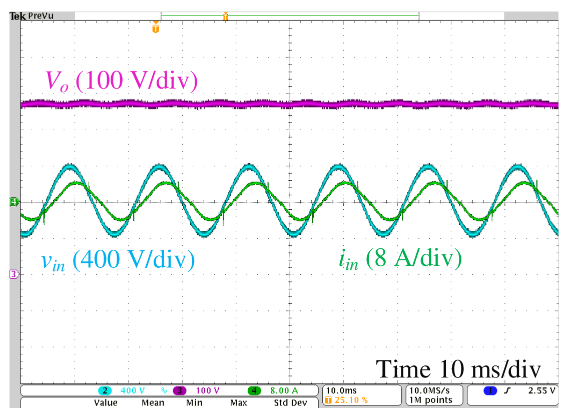

(c)

Fig. 12. Experimental waveforms of the GaN-based CRM T-type totem-pole rectifier prototype at (a) 0.94 lagging PF with $P = 1435$ W, $Q = 516$ VAr; (b) 0.79 leading PF with $P = 782$ W, $Q = -600$ VAr; (c) 0.87 lagging PF with $P = 779$ W, $Q = -431$ VAr when $v_{in} = 277\ \mathrm{V_{ac}}, V_o = 480\ \mathrm{V_{dc}}$.

capability of the rectifier prototype is validated at 0.94 PF, 0.87 PF, and 0.79 PF, and the tested efficiency is above 98.5%.

Acknowledgment

This work made use of the Engineering Research Center Shared Facilities supported by the Engineering Research Center Program of the National Science Foundation and DOE under NSF Award Number EEC-1041877 and the CURENT Industry Partnership Program.

References

[1] S. R. Islam, S. Maxwell, M. K. Hossain, S. Y. Park, and S. Park, "Reactive power distribution strategy using power factor correction converters for smart home application," in *IEEE Energy Conversion Congress and Exposition (ECCE)*, 2016, pp. 1–6.

[2] C. Nie, Y. Wang, W. Lei, M. Chen, and Y. Zhang, "An enhanced control strategy for multiparalleled grid-connected single-phase converters with load harmonic current compensation capability," *IEEE Transactions on Industrial Electronics*, vol. 65, no. 7, pp. 5623–5633, 2017.

[3] D. Xiao, M. Chen, and Y. Chen, "Negative sequence current and reactive power comprehensive compensation for freight railway considering the impact of DFIGs," *CPSS Transactions on Power Electronics and Applications*, vol. 6, no. 3, pp. 235–241, 2021.

[4] J. Dixon, L. Moran, J. Rodriguez, and R. Domke, "Reactive power compensation technologies: State-of-the-art review," *Proceedings of the IEEE*, vol. 93, no. 12, pp. 2144–2164, 2005.

[5] S. K. Mondal, "Active and reactive power compensation of data center using multi-level STATCOM inverter," in *IEEE International Symposium on Power Electronics for Distributed Generation Systems (PEDG)*, 2016, pp. 1–8.

[6] ABB, "PCS100 STATCOM-dynamic reactive power compensation, technical catalogue," https://library.e.abb.com/, 2014, [Online; accessed Dec-2020].

[7] J. Kueck, B. Kirby, T. Rizy, F. Li, and N. Fall, "Reactive power from distributed energy," *The Electricity Journal*, vol. 19, no. 10, pp. 27–38, 2006.

[8] USA Department of Energy, "Load participation in ancillary services workshop report," https://www.energy.gov/eere/analysis/downloads, 2011, [Online; accessed Dec-2020].

[9] S. M. Kaviri, M. Pahlevani, B. Mohammadpour, P. Jain, and A. Bakhshai, "Power control of a bi-directional ac/dc rectifier used for telecom backup systems," in *IEEE International Telecommunications Energy Conference (INTELEC)*, 2015, pp. 1–5.

[10] N. Akel, M. Pahlevaninezhad, and P. Jain, "A dq rotating frame reactive power controller for single-phase bidirectional converters," in *IEEE International Telecommunications Energy Conference (INTELEC)*, 2014, pp. 1–5.

[11] L. Liu, H. Li, Y. Xue, and W. Liu, "Reactive power compensation and optimization strategy for grid-interactive cascaded photovoltaic systems," *IEEE Transactions on Power Electronics*, vol. 30, no. 1, pp. 188–202, 2014.

[12] R. Kabiri, D. G. Holmes, B. P. McGrath, and L. G. Meegahapola, "LV grid voltage regulation using transformer electronic tap changing, with PV inverter reactive power injection," *IEEE Journal of Emerging and Selected Topics in Power Electronics*, vol. 3, no. 4, pp. 1182–1192, 2015.

[13] M. A. Fasugba and P. T. Krein, "Gaining vehicle-to-grid benefits with unidirectional electric and plug-in hybrid vehicle chargers," in *IEEE Vehicle Power and Propulsion Conference*, 2011, pp. 1–6.

[14] S. M. Park and S.-Y. Park, "Versatile control of unidirectional ac-dc boost converters for power quality mitigation," *IEEE Transactions on Power Electronics*, vol. 30, no. 9, pp. 4738–4749, 2014.

[15] M. C. Kisacikoglu, M. Kesler, and L. M. Tolbert, "Single-phase on-board bidirectional PEV charger for V2G reactive power operation," *IEEE Transactions on Smart Grid*, vol. 6, no. 2, pp. 767–775, 2014.

[16] W. Song, Z. Deng, S. Wang, and X. Feng, "A simple model predictive power control strategy for single-phase PWM converters with modulation function optimization," *IEEE Transactions on Power Electronics*, vol. 31, no. 7, pp. 5279–5289, 2015.

[17] Q. Huang, R. Yu, Q. Ma, and A. Q. Huang, "Predictive ZVS control with improved ZVS time margin and limited variable frequency range for a 99% efficient, 130 W/in^3 MHz GaN totem-pole PFC rectifier," *IEEE Transactions on Power Electronics*, vol. 34, no. 7, pp. 7079–7091, 2018.

[18] J. Sun, H. Gui, J. Li, X. Huang, N. Strain, D. J. Costinett, and L. M. Tolbert, "Mitigation of current distortion for GaN-based CRM totem-pole PFC rectifier with ZVS control," *IEEE Open Journal of Power Electronics*, vol. 2, pp. 290–303, 2021.

[19] Z. Liu, "Characterization and application of wide-band-gap devices for high frequency power conversion," Ph.D. dissertation, Virginia Tech, 2017.

[20] B. Sun, "Control challenges in a totem-pole PFC," *Analog Appl. J.*, vol. 2, pp. 1–4, 2017.

[21] R. A. Siddique, R. Khandekar, P. Ksiazek, and J. Wang, "Investigation of zero-crossing common-mode noise and current spike in GaN based totem-pole PFC," in *IEEE Canadian Conference on Electrical and Computer Engineering (CCECE)*, 2018, pp. 1–5.

[22] J. Sun, X. Huang, N. N. Strain, D. J. Costinett, and L. M. Tolbert, "Inductor design and ZVS control for a GaN-based high efficiency CRM totem-pole PFC converter," in *IEEE Applied Power Electronics Conference and Exposition (APEC)*, 2019, pp. 727–733.

[23] J. Sun, "Data center power system emulation and GaN-based high-efficiency rectifier with reactive power regulation," Ph.D. dissertation, the University of Tennessee, Knoxville, 2022.